HiSST: 3rd International Conference on
High-Speed Vehicle Science Technology
14 -19 April 2024, Busan, Korea

Heat Transfer Characteristics of the Missile Radome Considering Flight Scenario

Sangbin Han[1], Hyung Mo Bae[2], Jihyuk Kim[3], Dongkyun Lee[4], Kyeongho Lee[5], Sunghwan Yim[6], and Hyung Hee Cho[7]

Abstract

The radome of a missile flying at supersonic or hypersonic speeds is subjected to an excessive heat flux due to aerodynamic heating, in which kinetic energy is converted into thermal energy in the boundary layer. When the temperature of the radome wall exceeds the material's operating temperature, a critical issue arises as it renders the radome ineffective. Therefore, accounting for aerodynamic heating is crucial in radome design. In reality, the velocity and altitude of a missile change continuously after launch, leading to variations in the heat flux experienced by the radome over time. Therefore, in this study, to ascertain the influence of changing velocity and altitude on radome heat transfer, results of transient numerical analysis assuming the missile cruises at a constant altitude were compared with results of quasi-transient method numerical analysis considering the flight scenario. When considering the flight scenario, significant differences were observed in the temperature of the radome wall, in-depth line, and internal flow. In particular, when cruising at Mach 7, the thermal margin calculation yielded 99.95%, whereas considering the flight scenario resulted in 0.019%, showing a difference of 99.93% between the two cases. Thus, this study contributes to understanding radome heat transfer characteristics considering flight scenarios, facilitating stable operation, and efficient radome design.

Keywords: *AERODYNAMIC HEATING, RADOME, FLIGHT SCENARIO, QUASI-TRANSIENT METHOD, THERMAL MARGIN*

Nomenclature

Latin
A – Area, m^2
c_P – Specific heat of air, J/kg·K
d – Wall thickness of radome, mm
M – Mach number
n – Natural number
r – Recovery factor
T – Temperature, K
t – Time, s
U – Velocity, m/s

Greek
α – Flight path angle, degrees
γ – Specific heat ratio of air
ε – Dielectric constant
λ – Wavelength, mm

Subscripts
aw – Adiabatic
w – Radome wall
s – Static
safe – Below operating temperature
t – Total
total – Radome total

[1] *Department of Mechanical Engineering, Yonsei Univ., Seoul, 03722, Korea, kevi06@yonsei.ac.kr*
[2] *Department of Mechanical Engineering, Yonsei Univ., Seoul, 03722, Korea, zzexe@yonsei.ac.kr*
[3] *Department of Mechanical Engineering, Yonsei Univ., Seoul, 03722, Korea, jihyuk@yonsei.ac.kr*
[4] *LIGNex1, Gyeonggi-do, 13488, Korea, dongkyun.lee@lignex1.com*
[5] *LIGNex1, Gyeonggi-do, 13488, Korea, kyeongho.lee@lignex1.com*
[6] *LIGNex1, Gyeonggi-do, 13488, Korea, shyim1031@lignex1.com*
[7] *Department of Mechanical Engineering, Yonsei Univ., Seoul, 03722, Korea, hhcho@yonsei.ac.kr*

$_{if}$ – Inner fluid ∞ – Mainstream

1. Introduction

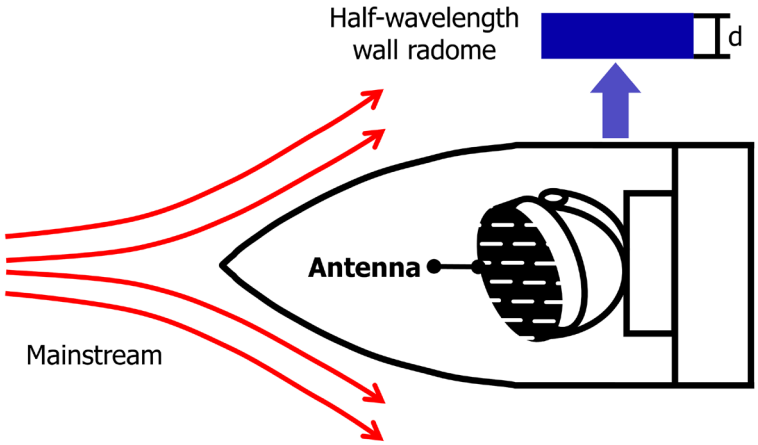

Fig 1. Schematic illustration of the half-wavelength wall radome and the missile antenna in supersonic or hypersonic flow.

The radome protects electronic equipment such as an antenna from the external environment at the tip of the missile[1]. Supersonic or hypersonic vehicles are exposed to an excessive heat flux due to aerodynamic heating caused by friction with the surrounding air. The temperature rises on the radome surface due to aerodynamic heating can affect the thermal stability of the radome and the performance of the antenna, necessitating prediction of the radome's thermal environment during the design of the radome[2].

Research on predicting the radome's thermal environment was conducted through experiments and numerical simulation. Dankert, C. et al.[3] validated the temperature of the radome wall within the Mach 6 flow field through a comparison between hypersonic wind tunnel test results and numerical simulation results. Hohn, O. et al.[4] analyzed the temperature of the radome wall through hypersonic wind tunnel experiments and investigated the influence of insulation materials inside the radome. Previous studies focused on the temperature distribution of the radome within a steady flow field without considering variations in velocity and altitude due to limitations in experimental devices.

The missile is operated under various scenarios, and the thermal load applied to the missile changes as the velocity and altitude continuously vary after launch. Therefore, it is necessary to predict the thermal environment of the radome through transient numerical analysis considering changes over time. To perform numerical analysis reflecting changes in velocity and altitude, a full transient analysis technique considering fluid flow variations over time is required. However, the time scale of supersonic or hypersonic turbulent flow is very small, making it impossible to perform a full transient analysis considering overall condition changes. Therefore, a loosely coupled method, which separates the flow and heat conduction of the missile, is generally applied[5]. The loosely coupled method fixes the temperature of the missile surface during convective heat transfer analysis, derives heat flux through steady heat flow field analysis, and applies this heat flux to transient conductive heat transfer analysis. However, it does not consider the decrease in heat flux over time as the surface temperature of the aircraft increases, resulting in excessive heat flux input compared to reality. Therefore, in this study, a quasi-transient analysis method combining the loosely coupled method and transient conjugate heat transfer (CHT) analysis was used[6]. Unlike the loosely coupled analysis method, the quasi-transient method performs conjugate transient heat transfer analysis, thus allowing for the reflection of changes in surface temperature and heat flux over time.

Therefore, this study applied the quasi-transient method to the missile radome, as depicted in Fig. 1, to compare the results considering the flight scenario with those obtained from transient analysis within a steady flow field. This was done to demonstrate the importance of considering flight scenarios in radome design. In addition, through the presentation of the thermal margin, meaningful design guidelines were proposed when designing the radome.

2. Research Method

2.1. Simulation domain

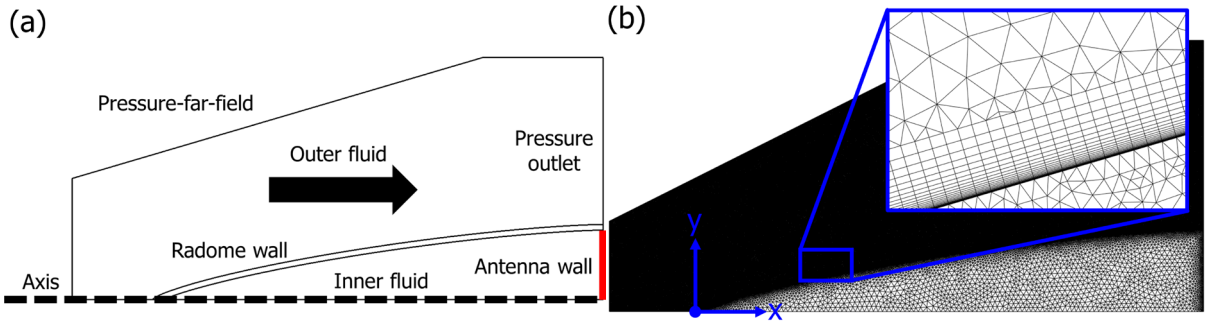

Fig 2. (a) Domain and (b) computational grids for numerical simulation of radome.

As for the radome shape of this study, the Von-Karman shape with excellent aerodynamic properties was selected. The length of the radome is 560 mm and the radius is 93.0 mm. The dimensions of the radome were referenced from the currently deployed air-to-air missile. To simplify the shape of the radome, the nose-tip at the tip of the radome and the junction between the missile fuselage were not considered. The axisymmetric two-dimensional simulation domain used in the numerical simulation is depicted in Fig. 2 (a).

Table 1. Properties of the radome material; Pyroceram 9606[7].

Density	2,610 kg/m^3
Specific heat capacity	821 J/kg·K
Thermal conductivity	4.08 W/m·K
Thermal diffusivity	1.904 mm^2/s
Softening temperature	1623.15 K
Dielectric constant	5.58

The material of the radome wall is Pyroceram 9606, which is commonly used in the production of the radome[8], and the properties used in the numerical simulation are listed in Table 1. Glass-ceramics such as Pyroceram 9606 reach their softening point and undergo material softening when heated, resulting in the loss of functionality as the radome. In this study, the softening temperature of Pyroceram 9606, which is 1623.15 K, was selected as the material's maximum operating temperature. The thickness of the radome wall was determined by selecting a half-wave wall structure, which is determined by the material's dielectric constant and the wavelength length of the radar frequency. The frequency of the radar was assumed to be 10 GHz, one of the X-band radar frequencies. The thickness of the radome wall derived by the Eq. 1 is 6.3 mm[9].

$$\mathrm{d} = \frac{n\lambda}{2\sqrt{\varepsilon}} \tag{1}$$

To verify the grid independence, the area average temperature of the mainstream at the same altitude was calculated for Mach number 7 using five different quantities of grids. The results shown in Fig. 3 indicate that the temperature variation of the mainstream is relatively small when the number of grids exceeds approximately 0.46 million. To reduce computing costs, the number of 0.46 million grids was chosen for numerical simulation. The grid used in this study is as shown in Fig. 2 (b), and the domain is divided by the triangular grid. The grid on the radome wall was refined y+ to 1 or less through inflation.

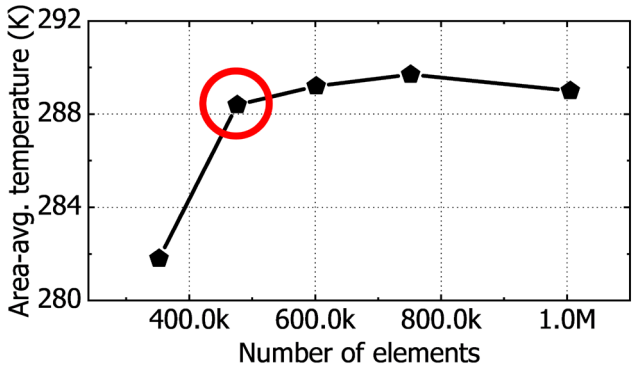

Fig 3. Verification of the grid independence.

2.2. Derivation of Flight Trajectory

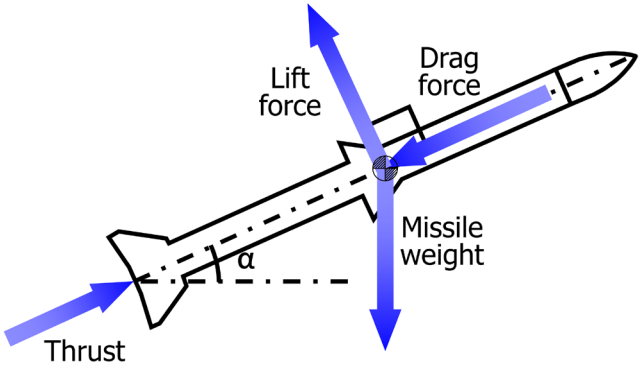

Fig 4. Schematic illustration of the forces that are exerted on a missile as files.

An in-house code was developed to derive the missile flight scenario. The chosen reference missile for scenario derivation was the U.S. AIM-120C-5 AMRAAM. Figure 4 illustrates the forces acting on the missile considered during the flight scenario derivation process. The flight scenario was computed using a 2-degree-of-freedom slender body model. The direction of thrust aligns with the missile's trajectory, while drag acts parallel to the direction of motion, and lift acts perpendicular to the direction of motion.

The variation in missile mass was calculated considering the amount of fuel consumed by the missile's propulsion system. The missile's thrust was determined based on the specific impulse of HTPB, the fuel used in the AMRAAM propulsion system. The drag force and lift force were calculated and reflected based on the AMRAAM's geometry, flight speed, and angle of attack.

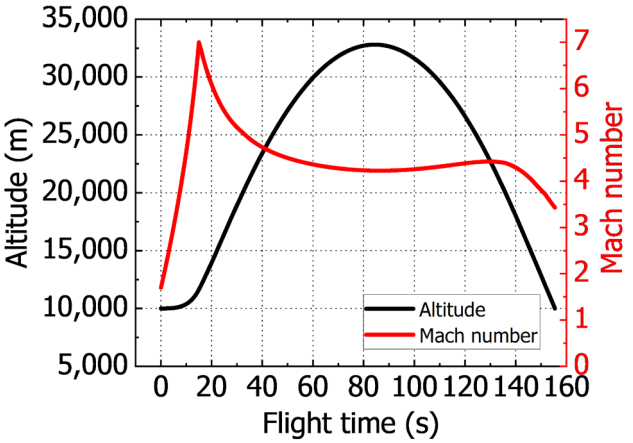

Fig 5. The altitude and Mach number of the missile flight scenario.

The missile flight scenario calculated through the code is depicted in Fig. 5. In the flight scenario of this study, the missile is launched from a virtual fighter flying at an altitude of 10,000 m at Mach number 1.7, and then the speed of the missile rises during a propulsion time of 15 seconds to reach the highest

speed of Mach number 7.0. Subsequently, it descends without thrust until it impacts the target upon reaching the initial altitude of 10,000 m, thus concluding the missile's flight at 155 seconds. As the missile's speed decreases after 15 seconds, it maintains a relatively stable flight speed, showing a slight increase, attributed to the gravitational force acting on the descending missile. As the missile's speed increases, so does the aerodynamic drag, leading to a subsequent decrease in speed after a certain time. The current AMRAAM missile does not reach Mach number 7.0, for thermal analysis purposes, the propulsion time was extended to assume a virtual missile reaching Mach number 7.0 as its maximum speed in a thermally problematic scenario.

2.3. Numerical Analysis Method and Boundary Conditions

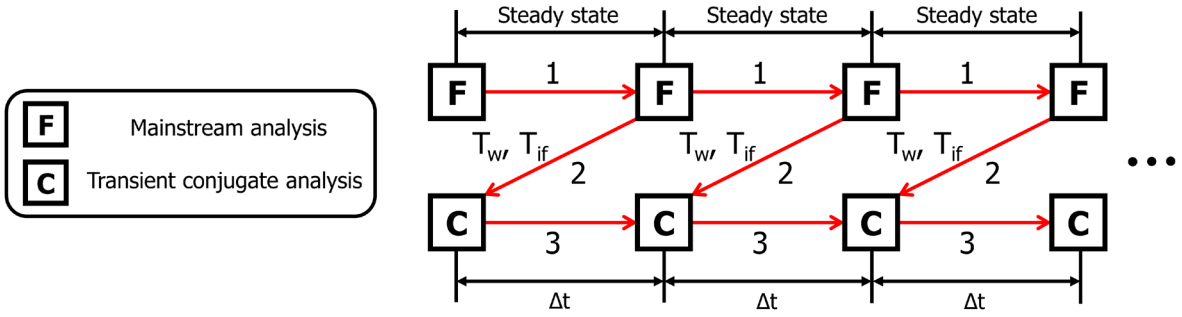

Fig 6. Strategy of Quasi-transient method analysis for the CHT problems in supersonic or hypersonic flows.

The quasi-transient method offers the advantage of performing numerical analysis for CHT problems on supersonic or hypersonic flows passing through flight bodies where transient analysis is infeasible due to computational limitations. Figure 6 illustrates how the quasi-transient method is performed. The quasi-transient method involves dividing a given flight scenario into multiple sections over time, performing steady flow field analysis and transient CHT analysis. In this study, a method was devised to divide the sections for steady flow field analysis and transient CHT analysis based on the total temperature over time. In consideration of the velocity and altitude of the missile over time, the total temperature for the perfect gas was obtained through Eq. 2. A division occurred when there was a temperature difference of 250 K.

$$T_t = T_s \times \left\{1 + M^2 \left(\frac{\gamma-1}{2}\right)\right\} \tag{2}$$

The procedure for performing the quasi-transient method for each section is as follows: Starting from an arbitrary section with start time t_1 and end time t_2, the steady flow field analysis is initiated by fixing the initial temperature of the radome wall as the mainstream's ambient temperature at t_1 and applying the initial flow conditions. This allows the supersonic or hypersonic flow field to converge. Following the steady flow field analysis, the wall conditions of the fluid domain and solid domain are coupled, and transient CHT analysis is conducted until t_2. Upon completion of the transient CHT analysis, the temperature of the radome wall and internal flow conditions at t_2 are derived. These are then applied to the subsequent section's steady flow field analysis, where transient CHT analysis is performed again, incorporating conductive and convective heat transfer. This process is repeated for each section.

2.4. Boundary conditions

In this study, ANSYS Fluent v.19.2 was used, utilizing a density-based solver advantageous for compressible flow analysis. The turbulence model was validated, and the SST k-ω model was selected. A second-order upwind scheme was applied for the discretization of each variable. The pressure far field condition was applied as the inlet condition of the flow, and the pressure outlet condition was applied as the outlet condition of the flow. To consider the temperature conditions of the antenna inside the radome, a constant temperature condition of 343.15 K was assigned to the antenna wall.

To reflect the flight scenario using the quasi-transient method, this study divided the sections to conduct the steady-state flow analysis and the transient CHT analysis based on total temperature over time. In consideration of the velocity and altitude of the missile over time, the total temperature was determined using Eq. 2, and sections were partitioned based on a temperature difference of 250 K. The segmented regions are depicted in Fig. 8, with the Mach number and altitudes for each section detailed in Table 2.

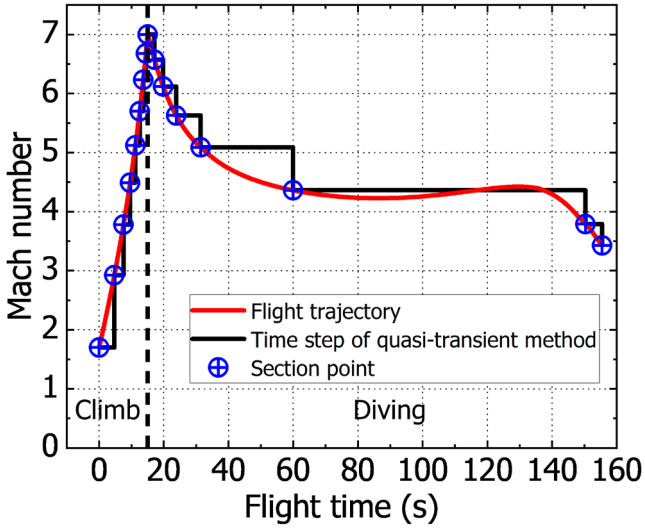

Fig 7. Flight scenario sections are divided by the total temperature difference of the mainstream.

Table 2. Flow conditions of flight scenario by section for quasi-transient method.

Step	Time	Mach number	Altitude
1	0.00 sec	1.7	10,000 m
2	4.71 sec	2.9	10,000 m
3	7.53 sec	3.8	10,300 m
4	9.59 sec	4.5	10,300 m
5	11.2 sec	5.1	10,600 m
6	12.6 sec	5.7	10,900 m
7	13.6 sec	6.2	11,200 m
8	14.5 sec	6.7	11,400 m
9	15.0 sec	7.0	11,600 m
10	17.1 sec	6.6	12,600 m
11	19.8 sec	6.1	13,900 m
12	23.8 sec	5.6	15,900 m
13	31.4 sec	5.1	19,600 m
14	59.9 sec	4.4	29,900 m
15	150 sec	3.8	12,700 m
16	155 sec	3.4	10,000 m

Table 3. Case summary for comparison of radome temperature distribution.

Case	Mach number	Altitude
Quasi-transient	Varies over time (Table 2)	Varies over time (Table 2)
Ma7.0_cruising	7.0	11,600 m
Ma3.4_cruising	3.4	10,000 m
Ma1.7_cruising	1.7	10,000 m

To compare and analyze the influence of flight scenarios on the heat transfer characteristics of the radome, four cases were selected as shown in Table 2. Numerical analyses were conducted for the "Quasi-transient" case, which reflects the flight scenario, and three "Cruising" cases assuming cruising at different altitudes with different Mach numbers. The atmospheric conditions of each case and each step were determined based on the "U.S. Standard Atmosphere, 1962." The cases analyzed in this study are listed in the table.

2.5. Validation of turbulence model

Heat transfer analysis within a supersonic or hypersonic flow is challenging due to the occurrence of aerodynamic heating at the boundary layer, making accurate predictions difficult. Therefore, to select the optimal turbulence model and wall function, turbulence models were validated. At the tip of the radome, there is a stagnation point where the flow velocity becomes zero, leading to the most significant manifestation of aerodynamic heating as the temperature recovers. In consideration of this, validation of heat flux within hypersonic flow fields for blunt bodies with stagnation points was conducted, and the results are depicted in Fig. 7. The k-ω SST turbulence model used in this study showed the lowest error of 13.9% at the stagnation point and relatively accurately predicted the trend of heat flux for blunt bodies.

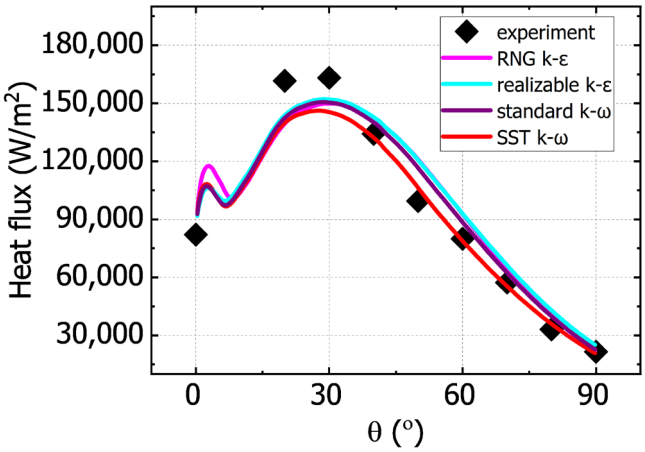

Fig 8. Comparison between predicted and experimental wall heat flux considering various turbulence models[6].

3. Results and Discussion

3.1. Quasi-transient case results

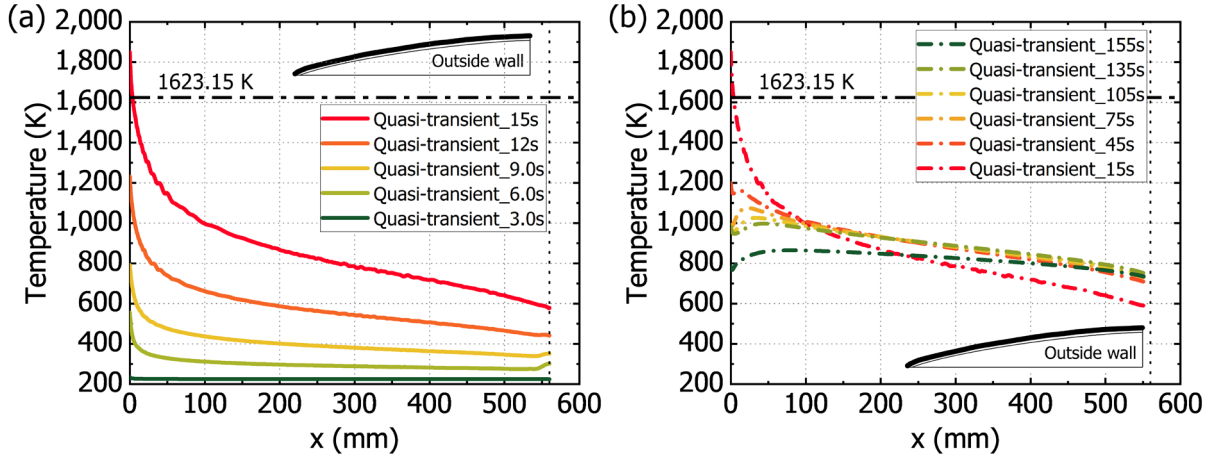

Fig 9. The time evolution of radome outer wall temperature distribution (a) with the flight time from 0 to 15 seconds and (b) 15 to 155 seconds.

Within supersonic or hypersonic flows, the temperature of an adiabatic wall is defined by Eq. 3, indicating that the temperature of the radome wall surface will be higher than the static temperature

of the mainstream. As the temperature rise is proportional to the square of the mainstream velocity, it can be expected that the magnitude of temperature change will increase to higher velocities.

$$T_{aw} = T_{\infty} + r\frac{U_{\infty}^2}{2c_p} \tag{3}$$

Figure 9 (a) shows the outer wall temperature of the radome when the quasi-transient method is applied from 0 to 15 seconds. During this period, as the missile accelerates, the overall outer wall temperature increases over time. The temperature of the radome's outer wall is highest at the tip and gradually decreases along the x-direction of the wall. This phenomenon occurs because the flow velocity becomes zero at the stagnation point of the tip (x=0 mm), resulting in intense heating close to the total temperature. Subsequently, as the boundary layer of the flow develops, the recovery coefficient decreases, leading to a decrease in the outer wall temperature of the radome. At 15 seconds, the temperature at the stagnation point reaches 1850 K, indicating that a portion of the outer wall exceeds the maximum operating temperature of Pyroceram 9606, which is 1623.15 K.

Figure 9 (b) shows the outer wall temperature of the radome when the quasi-transient method is applied from 15 to 155 seconds. During this period, as the missile decelerates, the temperature of the outer wall is partially reduced. However, in the lower part of the radome, despite being heated during acceleration, the temperature remains relatively constant during deceleration due to continued heating by the mainstream. Near the tip of the radome, the temperature decreases from 1850 K at 15 seconds to 780 K at 155 seconds, as the heat flux decreases with decreasing Mach number.

3.2. Comparing Quasi-transient case with cruising case

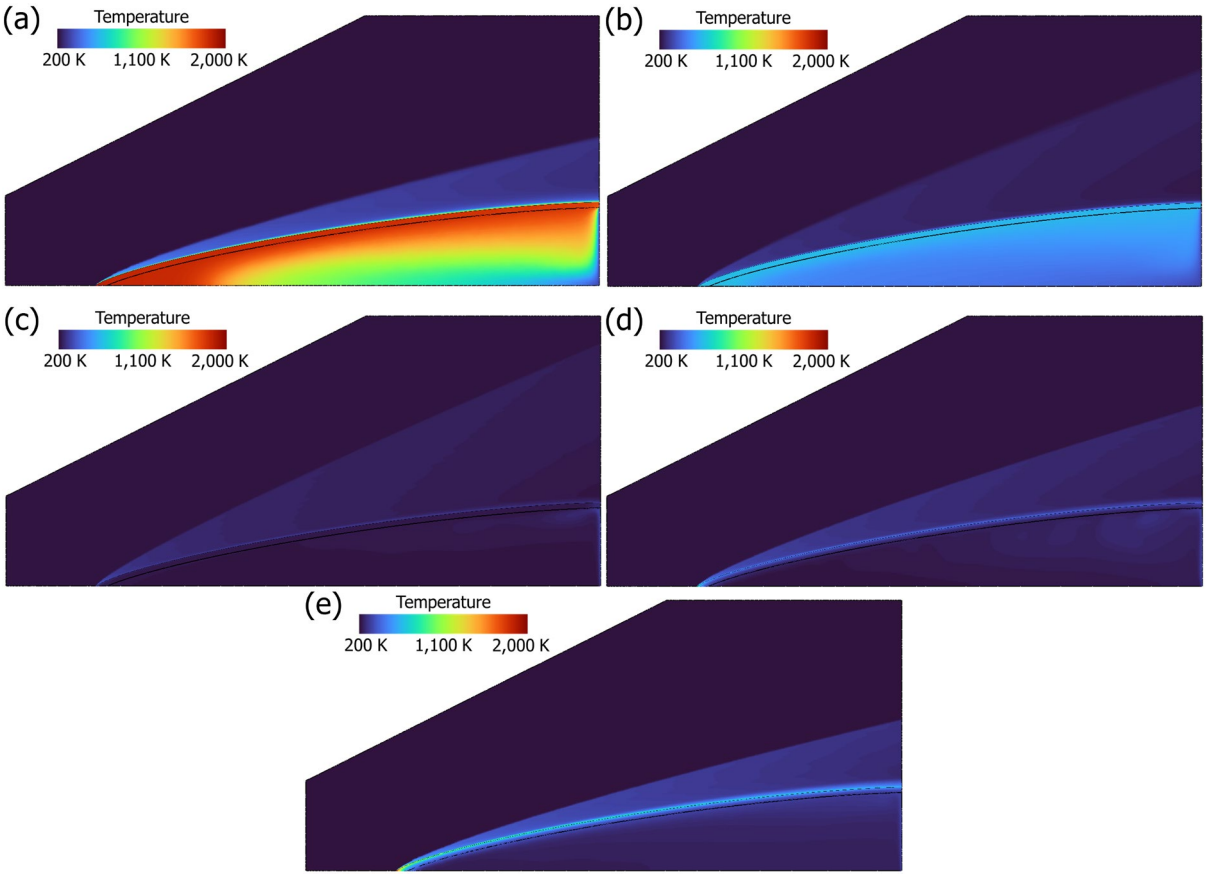

Fig 10. Contour of radome temperature by case: (a) Ma7.0_cruising case at 15 seconds. (b) Ma3.4_cruising case at 15 seconds. (c) Quasi-transient case at 5.0 seconds. (d) Quasi-transient case at 10 seconds. (e) Quasi-transient case at 15 seconds.

Figure 10 (a) illustrates the temperature contour after 15 seconds for the Ma7.0_cruising case, while Fig. 10 (b) shows the temperature profile after 15 seconds for the Ma3.4_cruising case. Additionally, Figs. 10 (c), (d), and (e) depict temperature contours at 5, 10, and 15 seconds, respectively, for the Quasi-transient case. In the Ma7.0_cruising and Ma3.4_cruising cases, due to the constant velocity and

altitude of the mainstream in the transient analysis, the angle of the shock wave remains unchanged. However, in the Quasi-transient case, the angle of the shock wave due to mainstream varies with changing velocity and altitude, reflecting changes in the flow field at each contour.

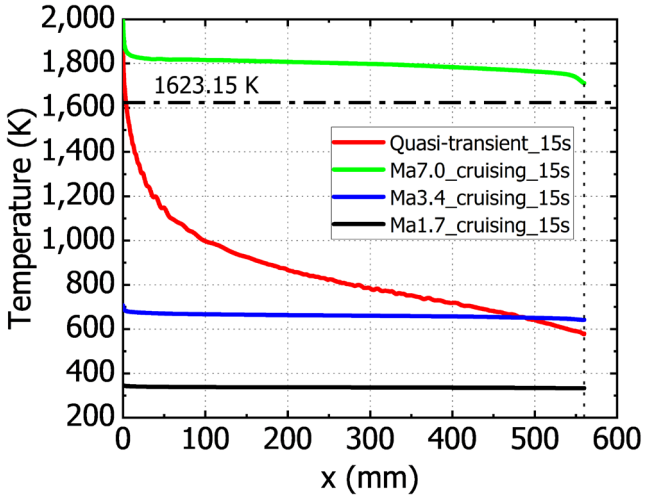

Fig 11. The comparison of the outer wall temperature distribution of the radome for each case at 15 seconds

To demonstrate the necessity of considering the flight scenario in radome design, comparisons were made between cases with and without the quasi-transient method applied. Figure 11 presents the outer wall temperatures of the radome at 15 seconds, after the completion of acceleration. At the stagnation point, the temperatures are 1850 K, 2000 K, 700 K, and 350 K in the quasi-transient, Ma7.0_cruising, Ma3.4_cruising, and Ma1.7_cruising cases, respectively. Notably, in the quasi-transient case, where varying velocities and altitudes are considered, the temperature distribution of the outer radome wall falls between 600 K and 1800 K, spanning from the highest velocity of Mach 7 to the lowest velocity of Mach 1.7. While the outer wall of the radome entirely exceeds the maximum operating temperature in the case of Ma7.0_cruising, only a portion near the stagnation point does so in the Quasi-transient case, indicating potential overestimation of aerodynamic heating effects when designing radomes based solely on the highest Mach number scenario.

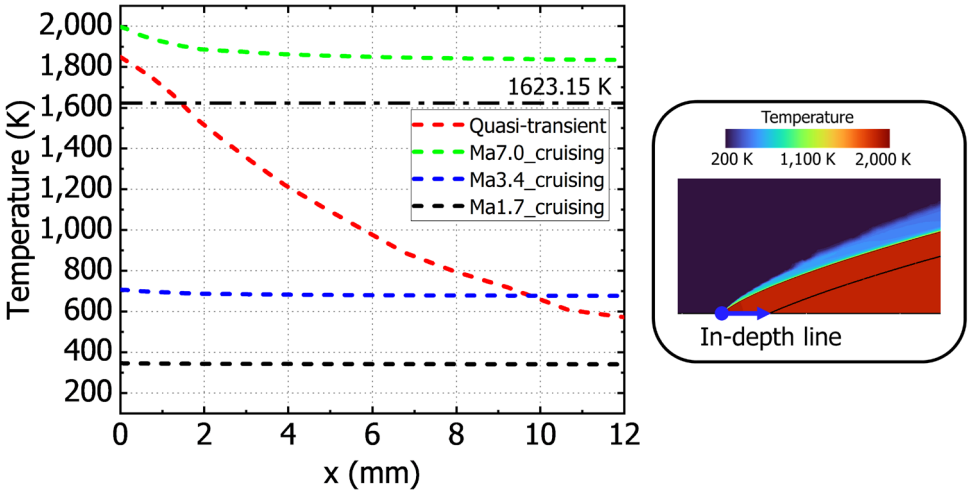

Fig 12. The comparison of the in-depth wall temperature of the radome for each case at 15 seconds.

The external surface of the radome, heated by supersonic or hypersonic flows, undergoes heat penetration into the interior over time due to conduction. To examine this influence, internal temperature distributions were compared across cases. Figure 12 depicts the temperature distribution within the stagnation point in-depth line at 15 seconds for each case. The peak temperatures within the radome wall match those of the outer wall. Similarly to the outer wall temperatures, the Quasi-transient case exhibits temperature distributions between those of the cruising cases. Furthermore, it

is observed that in the case of cruising at Mach 7, the entire interior of the wall is heated beyond the maximum operating temperature, whereas in the quasi-transient case, it is heated beyond the maximum operating temperature only up to 1.5 mm into the interior. This suggests that considering varying velocities and altitudes in radome design allows for the partial replacement of the wall material, preserving efficiency compared to a complete replacement necessitated by exposure during the highest Mach number scenario.

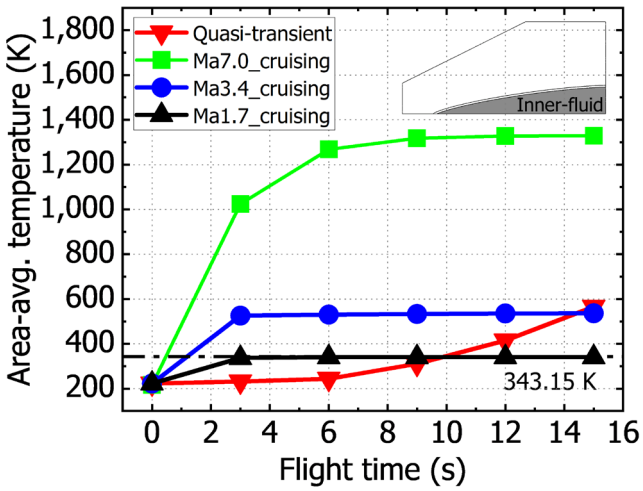

Fig 13. The comparison of the area average inner-flow temperature of the radome for each case at 15 seconds.

As the antenna inside the missile is an electrical component, it fails to function properly when exposed to temperatures exceeding a certain threshold[2]. Thus, antenna cooling systems must be designed considering the temperature of the inner flow during missile design. Figure 13 illustrates the time-dependent area average temperature of inner flow for each case. The temperatures converge to approximately 1300 K, 530 K, and 340 K for the Ma7.0_cruising, Ma3.4_cruising, and Ma1.7_cruising cases, respectively. Conversely, in the Quasi-transient case, the internal flow temperature increases above the optimal operating temperature of 343.15 K due to changes in mainstream conditions, emphasizing the need for cooling systems to maintain antenna functionality.

3.3. Thermal margin of the radome

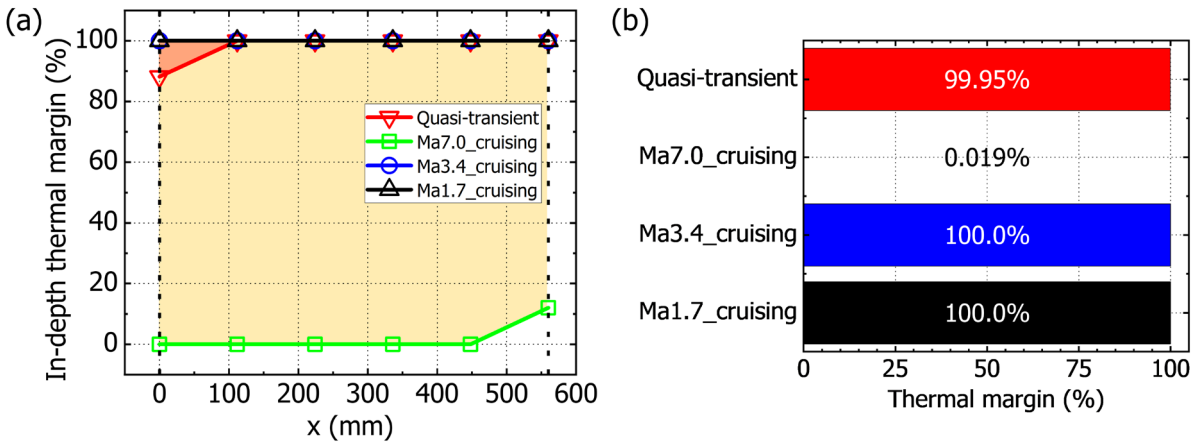

Fig 14. The comparison of thermal margins for each case at 15 seconds: (a) The thermal margin along the in-depth line of the radome wall at 6 points. (b) The thermal margin for the entire surface area of the radome.

In this study, the thermal margin was defined by Eq. 4 to evaluate the thermal stability of the radome. The thermal margin is the length or area below the melting point divided by the total length or area. If the thermal margin value reaches 100%, it indicates that the entire portion of the radome remains thermally stable and below the operating temperature of the material. If the material is heated above

its operating temperature, it may fail to function as the radome, potentially leading to issues under such conditions.

$$\text{Thermal margin} = \frac{A_{safe}}{A_{total}} \tag{4}$$

Figure 14 (a) depicts the thermal margin at six points along the x-direction of the inner wall for each case. The red-shaded areas indicate regions where the temperature exceeds the operating temperature in the quasi-transient case, while the orange-shaded areas represent regions exceeding the operating temperature in the Ma7.0_cruising case. For the Ma3.4_cruising and Ma1.7_cruising cases, the thermal margin is 100% across all regions, suggesting that the radome in this study is unlikely to encounter issues under these conditions. However, in the Ma7.0_cruising case, only the 560 mm point has a thermal margin of 12%, indicating that most areas experience heating above the operating temperature, rendering the radome unusable under this condition. The quasi-transient case shows an 88% thermal margin at the 0 mm point and a 100% thermal margin at other points. While some regions exceed the operating temperature, incorporating structures with high-operating temperature materials, such as nose-tips in the leading edges, may allow the radome to be used under this condition.

Figure 14 (b) illustrates the overall thermal margin for each case. The quasi-transient case has a thermal margin of 99.95%, but when cruising at Mach 7.0, the thermal margin decreases to 0.019%, indicating an excessive prediction of the radome temperature distribution when considering only cruising conditions.

4. Conclusions

In this study, the radome thermal environment considering the flight scenario was presented by applying a quasi-transient method to aid in providing thermal guidelines for radome design. To derive a hypothetical air-to-air missile flight scenario, an in-house code was developed. The resulting flight trajectory exhibited a maximum Mach number of 7.0 and a maximum altitude of 32,500 m. Based on this, sections suitable for applying the quasi-transient method were classified based on the mainstream's total temperature. Additionally, three cases were selected for comparison with the transient analysis results of a steady flow field.

For the quasi-transient method case and the transient analysis case of a steady flow field, the temperature of the outer wall of the radome, the temperature from the stagnation point to the inner wall, and the area average temperature of the inner flow were evaluated. Through the comparison of each case, it was confirmed that the result of the quasi-transient method case exists between the highest and lowest temperatures of the transient analysis case of a steady flow field. Furthermore, thermal margins that could be considered in the radome design were presented and compared for each case. A significant difference of 99.93% in the area thermal margin was identified between the case with the maximum Mach number and the case considering the flight scenario. The study results indicate that designing the radome based solely on transient analysis within a steady flow field may lead to considerable discrepancies in the temperature distribution compared to reality, highlighting its inefficiency. Thus, it is crucial to analyze the thermal environment of the radome considering flight scenarios. The presented quasi-transient method can be utilized to compute the thermal environment of the radome wall in a given flight scenario. Moreover, it provides a theoretical temperature range to ensure reliable performance of the radome by interpreting its thermal environment considering flight scenarios.

References

1. Crone, G.A.E., Rudge, A.W., Taylor, G.N. Design and performance of airborne radomes: A review. In IEE Proceedings F (Communications, Radar and Signal Processing). 128(6), 451-464 (1981)
2. Dhumal, A.R., Kulkarni, A.P. Ambhore, N.H. A comprehensive review on thermal management of electronic devices. Journal of Engineering and Applied Science. 70(140), (2023)
3. Dankert, C. Otto, H. Experimental Investigation and Numerical Simulation on a Missile Radome at Mach 6. In New Results in Numerical and Experimental Fluid Mechanics VI:

Contributions to the 15th STAB/DGLR Symposium Darmstadt, Germany. 317-232 (2007)

4. Hohn, O., Esser, B., Klevanski, J., Gülhan, A., Fener, R., Panthen, B., Frieß, M. Experimental Investigations for the Thermal Qualification of High Speed Missile Radomes. 8th European Conference for Aeronautics and Space Sciences (EUCASS), Madrid, Spain. 1-4 (2019)
5. Zhang, S., Chen, F., Liu, H. Time-adaptive, loosely coupled strategy for conjugate heat transfer problems in hypersonic flows. Journal of Thermophysics and Heat Transfer. 28(4), 635-646 (2014).
6. Bae, H.M., Kim, J., Bae, J.Y., Jung, D., Cho, H.H. Quasi-Transient Method for Thermal Response of Blunt Body in a Supersonic Flow. Journal of the Computational Structural Engineering Institute of Korea. 30(6), 495-500 (2017)
7. Salmon, D.R., Brandt, R., Tye, R.P. Pyroceram 9606, A certified ceramic reference material for high-temperature thermal transport properties: part 2—certification measurements. International Journal of Thermophysics. 31, 355-373 (2010)
8. Stookey, S.D. History of the Development of Pyroceram. Research Management. 1(3), 155-163 (1958)
9. Sunil. S., Venu, K.S., Vaitheeswaran, S.M., Raveendranath, U. A modified expression for determining the wall thickness of monolithic half wave radomes. Microwave and optical technology Letters. 30(5), 350-352 (2001)